J Mater Sci (2009) 44:976–984
DOI 10.1007/s10853-008-3210-0

Measurement of strain distributions near the steel/epoxy interface by micro-Raman spectroscopy under tensile load condition

Makoto Imanaka · Rika Ishikawa · Yoshiaki Sakurai · Koichi Ochi

Received: 1 July 2008 / Accepted: 19 December 2008 / Published online: 13 January 2009

Abstract Micro-Raman spectroscopy was applied for evaluating the stress distributions in the vicinity of the interface of the steel/epoxy bonded joint under tensile loading condition. Herein, single-walled carbon nanotubes (SWNTs) embedded in a polymer can be used as a mechanical sensor, in which the position of the D^* Raman band varies with the strain or stress transferred to SWNTs from the surrounding matrix. In order to evaluate the strain distributions, however, it is required to elucidate the effect of the multiaxial stress on the D^* band shift, because a multiaxial stress field appears in the vicinity of the interface and, the validity of this method has been confirmed only under uniaxial loading condition. Hence, at first, the D^* band shift of a bulk epoxy/SWNT composite was measured under biaxial loading condition using a cruciform-type specimen. It was found that the D^* band shift could be standardized in terms of the strain in the polarized direction even though under the biaxial condition. Then, on the basis of the result, this method was applied for evaluating the strain distributions of the steel/SWNT composite bonded joints under uniaxial tensile loading condition. The observation indicated that the strain singularity appeared in the vicinity of the interface, similar to the results of the finite-element analysis, and the observed strain almost agreed with calculated one in the range of 0.03–10 mm distance from the interface.

M. Imanaka (✉) · R. Ishikawa
Department of Technology Education, Osaka University of Eduction, Asahigoaka, Kashiwara, Osaka 582-8582, Japan
e-mail: imanaka@cc.osaka-kyoiku.ac.jp

Y. Sakurai
Department of Chemistry and Environment Technology, Technology Research Institute of Osaka Prefecture, Izumi, Osaka 594-1157, Japan

K. Ochi
Faculty of Chemistry, Material and Bioengineering, Kansai University, Suita, Osaka 564-8680, Japan

Introduction

Metal/polymer bonded materials have been widely used as adhesive joints, electrical devices, and so on in many engineering fields. For improving the reliability of the bonded materials, the accurate estimation of the bonding strength is required**.** In the vicinity of the metal/polymer interface, however, the stress singularity appears, which affects the bonding strength [1, 2]. Thus, many studies have been conducted on the stress analysis in the vicinity of the interface [3, 4]. The stress singularity field is extremely localized in the vicinity of the interface: normally within about 0.3 mm distance from the metal/polymer interface. To measure the stress distribution in the stress singularity field, the spatial resolution of the sensor to be used should be less than 0.01 mm; hence, strain gages cannot utilize the measurement because of the resolution of 0.2 mm at the most.

There are only a few studies on the experimental measurement of stress or strain distribution in the vicinity of the interface due to the difficulties. In such a situation, strain field near the interface has been measured only by Moiré interferometry, where strain distributions are derived through a differentiation operation of the observed fringe pattern corresponding to the displacement contour. Moreover, the measurement is limited in the adhesive layer of adhesively bonded lap joints under shear loading condition [5], and the detailed distribution in the singularity field has not been presented due to lack of the spatial resolution.

Recently, micro-Raman spectroscopy has been used for measuring the local strain distribution of polymeric materials containing dispersed single-walled carbon nanotubes (SWNTs) as mechanical sensors, wherein the Raman shift of nanotubes can be used for quantifying the strain or stress transferred to nanotubes from the surrounding matrix [6–15]. The observed Raman shift directly corresponds to the strain averaged in the laser spot whose size governs the spatial resolution; moreover, it is not difficult to focus on the specimen with a laser spot of 0.01 mm in diameter. Thus, the spatial resolution for the micro-Raman measurement is superior to that for the Moiré interferometry. To apply the measurement method for the evaluation of strain or stress in the vicinity of the metal/polymer interface, it is required to elucidate the effect of multiaxial stress on the Raman shift. Because the multiaxial stress field appears in the vicinity of the interface owing to the constraint of the metallic material, even though under the uniaxial loading condition.

In the present situation, the validity of the measurement method is confirmed only under uniaxial loading condition; hence to elucidate the effect of multiaxial stress on the Raman shift, we measured the Raman spectra of a bulk epoxy/SWNT composite under biaxial stress condition using a cruciform-type specimen. As a result, it was confirmed that there is a linear relationship between the D^* band shift and the strain in the polarized direction even though under the biaxial stress condition. With this finding, the Raman method was used to evaluate the strain distributions near the interface of a steel/SWNT composite joint specimen under a tensile loading condition. The measured strain distributions were compared with those calculated by the finite-element analysis. It was found that the measured strain distributions substantiate the stress singularity field in the vicinity of the interface similar to the calculated distribution, and almost agree with the calculated one in the range of 0.03–10 mm distance from the interface.

Experimental procedure

The SWNTs used in this study were provided by Stream Chemicals Inc. in USA. The SWNTs were suspended in ethanol and placed in a sonic bath for 2 h. Then, an epoxy resin (Epikote 828) was added to the mixture, which was sonicated for 0.5 h before being left in a vacuum oven for 24 h at 353 K to remove the residual ethanol. Finally, the mixture contained 0.1 wt% SWNT. After adding 25 phr of polyamine (HY560) as a curing agent, the mixture was stirred for 5 min in a vacuum chamber to remove air bubbles, then casted on three types of Teflon frame to prepare two types of bulk and one steel/SWNT composite joint specimen, and finally cured for 4 h at 373 K.

The bulk specimen with dimensions of 10 mm × 50 mm × 0.4 mm and the steel/SWNT composite joint specimen were used for the measurement by Raman spectroscopy under uniaxial tensile loading condition, where the steel plate used in this experiment was a tool steel (JIS SK5), and the bonding surface of the steel plate was treated by grit blasting using alumina grits. On the other hand, the Raman spectroscopy for the cruciform-type bulk specimen was carried out under biaxial loading condition. The shape and sizes of the steel/SWNT composite joint and cruciform-type bulk specimens are given in Fig. 1a and b, respectively, wherein the locations of the pasted strain gages are also indicated. To obtain stress–strain curves for the bulk SWNT composite and the epoxy resin without SWNTs, tensile tests for each bulk specimen were also conducted using dumbbell type (JIS K7113) specimen, where these tests were carried out on a universal testing machine (Shimadzu: Autograph 5000) at the 1 mm/min crosshead speed.

To measure the Raman spectra under tensile load conditions, a mini-tensile loading machine was attached onto a stage of a Reinshaw micro-Ramanscope, where the Raman spectra were obtained in the 180° backscattering geometry

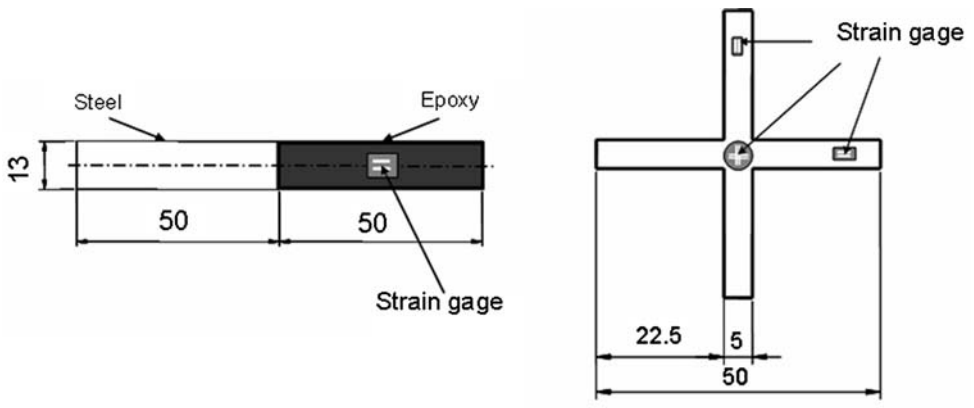

(a) Steel/epoxy joint specimen (Thickness t=0.4mm) (b) Cruciform-type specimen (Thickness t=0.4mm)

Fig. 1 Shape and dimensions of the specimens

with the 632.8 nm line of a 25 mW HeNe laser, and a charged-coupled device (CCD) has used as a detector. A polarized laser beam was focused onto the sample surface through a 20× objective lens, wherein the spot size was approximately 10 μm. The band positions of the spectra were calculated by curve fitting using a Gaussian routine.

Figure 2 shows a schematic drawing for the Raman spectra measurement of the steel/SWNT composite joint specimen under uniaxial loading condition, wherein the co-ordinate system is also indicated: the *X*-axis is parallel to the loading direction, and the origin of the co-ordinates is at the center of the specimen. The Raman spectra were recorded at different distances from the interface along the *X*-axis with various tensile strain levels that were monitored using the strain gages pasted on the specimen, as in Fig. 1a. The direction of the optical polarization agreed with the *X*-axis direction, i.e., the loading direction. The Raman spectra of the bulk specimen with rectangular section were recorded at the center of the specimen subjected to tensile strain of various levels, to obtain a calibration between strain and Raman shift.

Figure 3 shows a picture of cruciform-type specimen setup for Raman scattering measurement under bidirectional loading condition. To apply the *Y*-directional load to the specimen, a loading device using spring force was attached to the mini-tensile loading machine. The spectra were measured at the middle of the two-dimensional gage, wherein the strain gages attached on the arms were used to adjust the applied loads to the arms. The laser-polarized direction is also parallel to the *X*-axis.

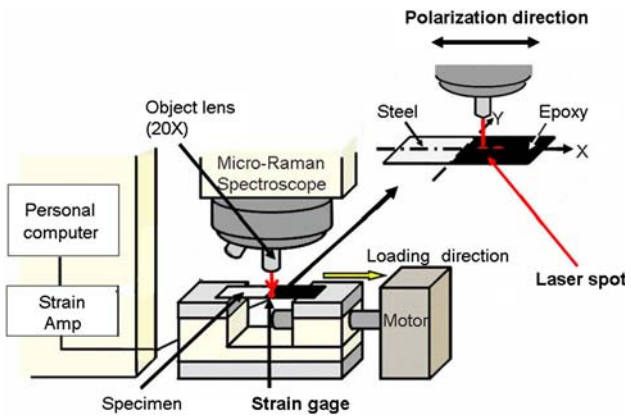

Fig. 2 Schematic of the steel/epoxy joint specimen setup for Raman scattering measurement under uniaxial loading condition

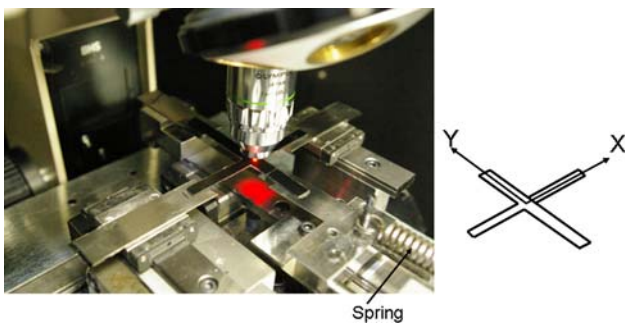

Fig. 3 Picture of cruciform-type specimen setup for Raman scattering measurement under bidirectional loading condition

Results and discussion

Mechanical properties of SWNT/epoxy composite

To determine the mechanical properties of the SWNT/epoxy composite, tensile tests were conducted using dumbbell-type specimens mentioned above. Figure 4 shows the stress–strain curves of the SWNT/epoxy composite and the epoxy resin without SWNTs. Young's modulus of both the resins can be obtained from the gradients of the curves in the elastic region. Moreover, Poisson's ratio was also measured using a two-dimensional strain gage. The mechanical properties of the SWNT/epoxy composite are listed in Table 1, which will be used for the stress analysis of the steel/epoxy joint specimens.

Young's modulus increases through the addition of SWNTs, whereas the breaking strain decreases a little, as in Fig. 4**.** Here, a comparison is made with a role-of-mixture type prediction of the Young's modulus of the SWNT/epoxy composite. Krenchel's model has been widely applied to three-dimensional randomly dispersed short-fiber composites [16],

$$E_{\mathrm{com}} = \eta E_{\mathrm{ep}} f_{\mathrm{ep}} + E_{\mathrm{cnt}} f_{\mathrm{cnt}} \tag{1}$$

which was also applied for the prediction of Young's modulus of several type of CNT/epoxy composites [17]. In

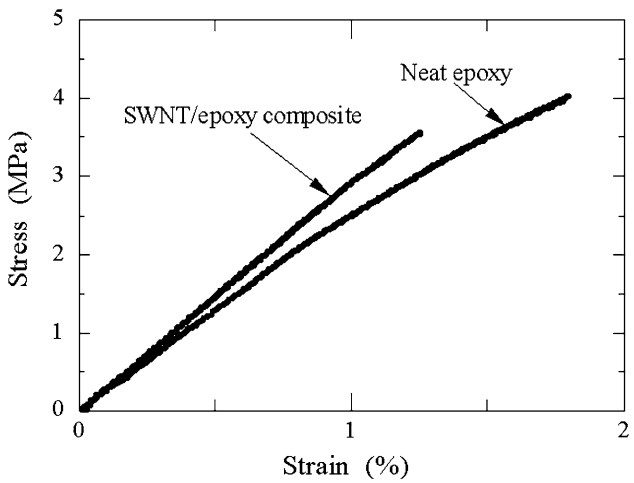

Fig. 4 Stress–strain curves for the bulk SWNT/epoxy composite and neat epoxy resin

Table 1 Material constants of the epoxy composite and steel used for stress analysis

	Young's modulus (GPa)	Poisson's ratio	Coefficient of thermal expansion
SMNT/epoxy composite	2.8	0.4	3.0×10^{-5}
Steel	206.0	0.33	1.2×10^{-5}

Eq. 1, f is the volume fraction (the subscript com, ep, and cnt denote composite, epoxy, and nanotube, respectively), and η is Krenchel's coefficient, which is 0.2 for three-dimensional randomly orientated rods [16]. We assumed that the nanotube modulus was 1 TPa, similar to Fidelus et al. [17]. Young's modulus of the matrixphase, $E_{ep} = 2.45$ GPa, was calculated from the stress–strain curve of the epoxy resin without SWNTs. The volume fractions of the nanotube and the epoxy matrix phase were calculated from the mass fractions using densities of the nanotube, $\rho_{cnt} = 1.4$ g/cc, and the matrix phase, $\rho_{ep} = 1.18$ g/cc. With these values, we obtained Young's modulus of the SWNT/epoxy composite to be 2.62 GPa, whereas the experimental value is 2.80 GPa (see Table 1). The experimental result higher than the estimated one means that the load is transferred efficiently from the matrix to the SWNTs. Fidelus et al. [17] also reported that the experimental Young's modulus for 0.05 wt% SWNTs was higher than the estimated one.

Raman spectra of bulk specimen under uniaxial loading condition

The Raman spectrum of SWNT has four main features: *G* band (centered at approximately 1,600 cm^{-1}), *D* band (at approximately 1,300 cm^{-1}), *D** band (at approximately 2,600 cm^{-1}), and the radial breathing mode (*centered* at approximately 180 cm^{-1}). Figure 5 shows the Raman spectra of SWNT powder, neat epoxy resin, and SWNT/epoxy composite. The clearest peak of the SWNT powder is the *G* band, but the epoxy resin also has several peaks at approximately 1,600 cm^{-1}. The neat epoxy resin has no Raman-active vibration mode in the vicinity of the *D** band. Hence, the *D** band has been used to monitor the strain or stress of SWNT embedded in the several types of polymer under uniaxial tensile loading condition within the elastic region [7–11, 14, 15], wherein the strain or stress dependence of the *D** band shift is related to the orientation of the SWNT and the polarized direction. In the case that the dispersion of the SWNTs in the polymer was incomplete, *D** band did not appear or revealed unclear peak. Thus, sharpness of the *D** band reflects the dispersion of the SWNTs; in other words, it is difficult to measure the *D** band for the sample whose dispersion was not complete.

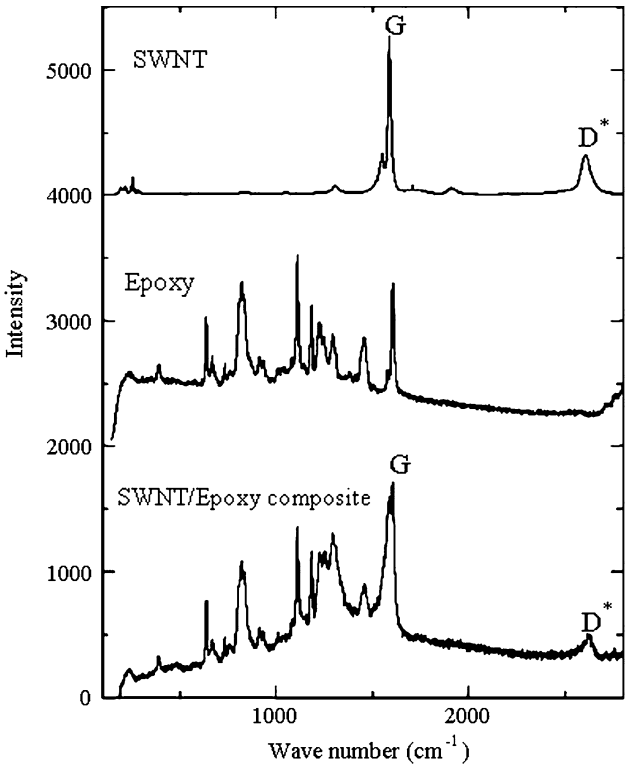

Fig. 5 Raman spectrum of SWNT powder, epoxy resin and SWNT/epoxy composite

When the SWNTs are aligned in the loading direction, the strain or stress sensibility of the *D** band shift has the highest value. However, the preparation of oriented SWNT composites is difficult. Recently, it was shown that the *D** band shift of SWNTs unorientated in a polymeric material is proportional to the tensile strain whose direction is parallel to the polarized one under uniaxial tensile loading condition, being also confirmed by theoretical calculation [9]. This indicates that unoriented SWNTs can be utilized as strain or stress sensors using polarized light.

Figure 6 shows the *D** band shift of the SWNT/epoxy composite as a function of tensile strain applied to the bulk specimen with rectangular section, wherein the *D** band shift was observed in the two polarized directions parallel and perpendicular to the loading ones in the elastic region. The Raman shift in the direction parallel to the loading decreases linearly with increasing strain. In the direction perpendicular to the loading, on the other hand, the Raman shift increases slightly with increasing strain. Such a trend agrees with the results of Frogley et al. [9].

Raman spectra of strain level under biaxial loading condition

As mentioned in Sect. Introduction, a multiaxial stress field appears in the vicinity of the interface of the steel/SWNT

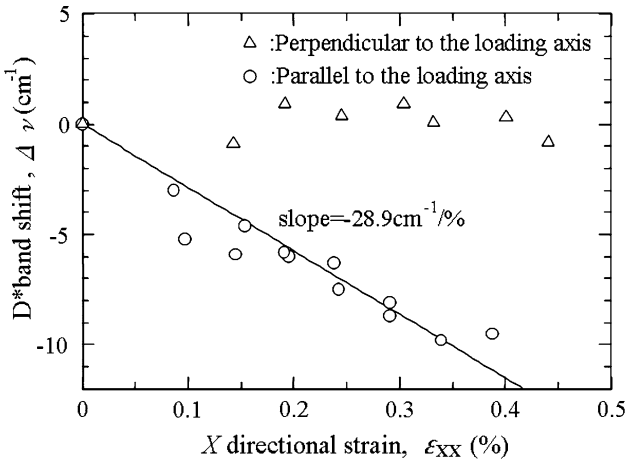

Fig. 6 D^* band shift of SWNT/epoxy composite, as a function of tensile strain

composite joint specimen owing to the constraint of the steel substrate, even under uniaxial loading condition. Under the uniaxial tensile loading condition, it has been confirmed that the D^* band shift can substantiate the strain or stress whose direction is parallel to the polarized one. However, it has not been reported that the D^* band shift is also proportional to the tensile strain or stress under multiaxial loading conditions. Besides, the stress state on the measured points is biaxial even though a triaxial stress state appears in the inner part of the specimen, because Raman spectra measurements are limited on the surface of the specimens. Hence, for the evaluation of the strain in the vicinity of the interface for the steel/SWNT composite joint specimens, it is sufficient only to elucidate the effect of stress biaxiality on the D^* band.

Here, we measured the D^* band shift under biaxial stress condition, using the cruciform-type specimen shown in Fig. 1b. Figure 7 shows the biaxial stress states at the measured point of the specimen. Under the assumption of the plain stress condition, X- and Y-directional stresses, σ_{XX} and σ_{YY}, were calculated from X- and Y-directional strains, ε_{XX} and ε_{YY}, respectively, detected with the two-dimensional strain gage pasted in the middle of the specimen as follows:

$$\sigma_{XX} = \frac{E}{1-\nu^2}(\varepsilon_{XX} + \nu\varepsilon_{YY})$$
$$\sigma_{YY} = \frac{E}{1-\nu^2}(\varepsilon_{YY} + \nu\varepsilon_{XX}) \quad (2)$$

where E and ν are Young's modulus and Poisson's ratio, respectively. As Fig. 7 shows, the biaxial stress state at the measured point ranges from uniaxial to equibiaxial stress states, which covers the stress biaxiality appeared in the vicinity of the interface.

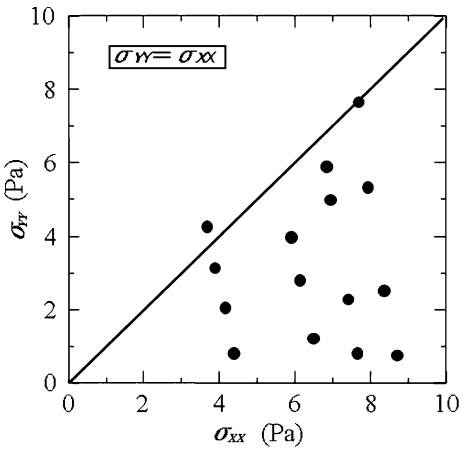

Fig. 7 Stress state of the measured point under biaxial stress condition

To confirm the strain uniformity within the strain gage, three-dimensional finite-element analysis was conducted for the SWNT composite that was treated as an elastic solid with material constants given in Table 1. Figure 8a shows an example of contour plots of the X-directional strain, ε_{XX}, in the middle part of the specimen. Although ε_{XX} gradually increases by approaching to the center of the specimen, these values are uniformly distributed within the range of the pasted gage (see Fig. 8b).

Under uniaxial loading condition, the stress in the loading direction is proportional to the strain. Hence, both stress and strain can be estimated from the D^* band shift. On the other hand, a linear relationship between stress and strain does not exist under biaxial stress condition. It is necessary to clarify which component should be used for the calibration plot of the D^* band shift under the biaxial stress condition. Figure 9a and b show the plots of D^* band shifts under biaxial stress condition against the X-directional stress and strain, respectively. The plots in terms of the stress are widely scattered and there is a considerable discrepancy between biaxial and uniaxial plots (see Fig. 9a). On the other hand, the plots in terms of the strain are well standardized and also agree with the uniaxial plots as in Fig. 9b. This indicates that the D^* band shift can be used for evaluating the strain parallel to the polarized direction even under the biaxial stress condition.

Raman spectra of steel/epoxy joint specimen

To compare the measured strain distributions at the steel/SWNT composite interface with analytical ones, three-dimensional finite-element analysis was conducted. Figure 10 shows the finite-element model for the steel/SWNT composite joint specimen near the interface. Since the joint specimen is symmetric to $X = 0$ and $Z = 0$ axes, a quarter of the joint is modeled. The X-directional fixed

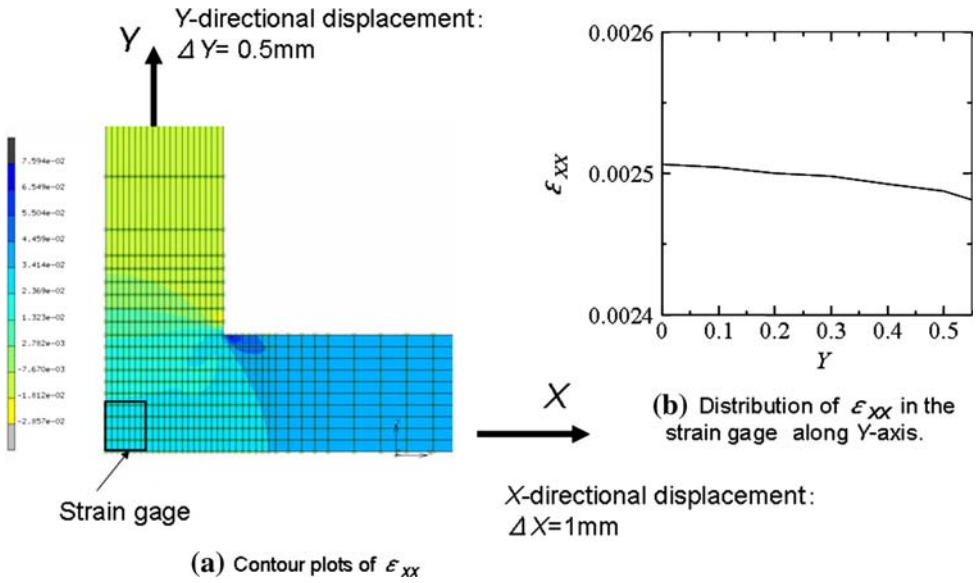

Fig. 8 Example of contour plots of ε_{XX} near the middle of the cruciform-type specimen and distribution in the strain gage

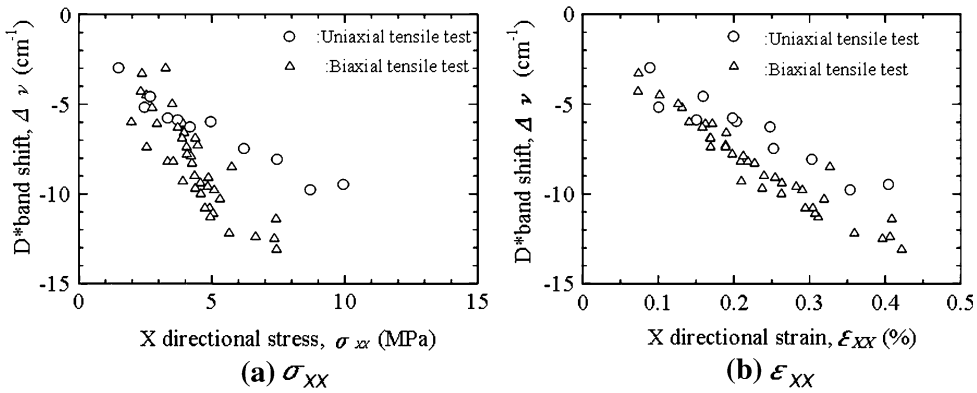

Fig. 9 D^* band shift versus X-directional stress or strain for the cruciform-type bulk specimens

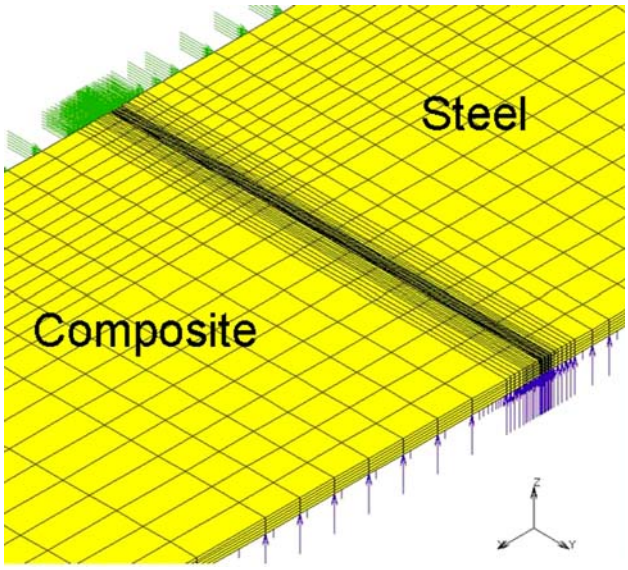

Fig. 10 Finite-element analysis model of the steel/SNWT epoxy composite joint

displacements of 0.1 mm are applied to the end of the steel plate, whereas X-, Y-, and directional displacements are fixed at the end of the SWNT composite. In this analysis, steel and SWNT composite substrates were treated as elastic solids with the material constants listed in Table 1. Owing to the difference in the thermal expansion coefficient between the steel plate and epoxy resin, residual stress appears near the interface during the cooling process at the curing temperature. The residual stress depends on $\Delta T = T_0 - T_{SF}$, where T_0 and T_{SF} are the room temperature (298 K) and stress-free temperature, respectively, and T_{SF} is lower than the curing temperature, T_{cure}. For the SWNT/epoxy composite, T_{SF} is unknown and the material constants vary with temperature. In this situation, the strict estimation of residual stress is very difficult, but the actual residual stress is lower than the calculated stress with $\Delta T_{max} = T_0 - T_{cure}$, which indicates a conservative estimation. Thus, the stress and strain distributions with $\Delta T_{max} = -75$ K are also calculated.

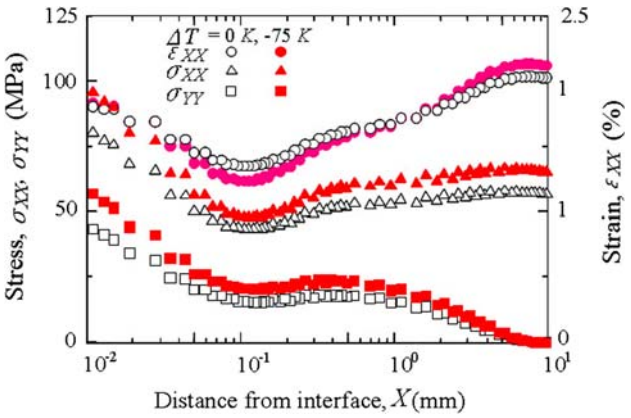

Fig. 11 σ_{XX}, σ_{YY}, and ε_{XX} distributions along the center of the specimen

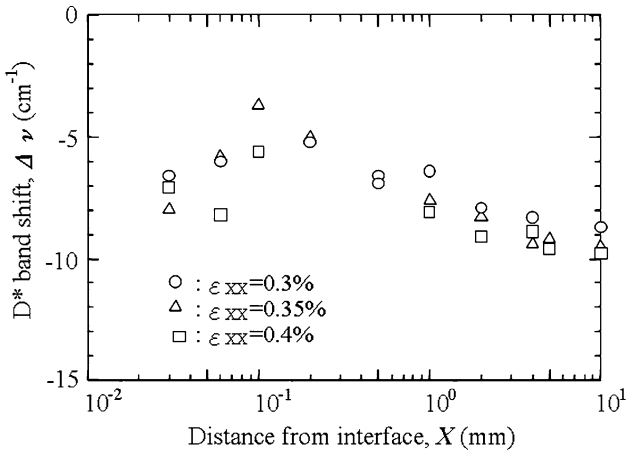

Fig. 12 Distributions of D^* band shift, Δv, along the center of the specimen

Figure 11 shows the distributions of X- and Y-directional stresses, σ_{XX} and σ_{YY}, and X-directional strain, ε_{XX}, along the center of the joint. Solid symbols represent the consideration of the cooling process at the curing temperature, open symbols doing no consideration. Irrespective of the cooling temperature, each stress or strain component diverges with the approach of the interface, because the stress singularity appears at the bonded interface under tensile loading condition. This figure also shows that σ_{XX} and ε_{XX} have minimum points near $X = 0.1$ mm, then become close to each uniform value at approximately $X = 2$ and 5 mm, respectively. On the other hand, σ_{YY} increases monotonically with the approach of the interface from $X = 5$ mm, owing to the constraint of the steel plate. When the stress and strain distributions are compared between $\Delta T = 0$ K and -75 K, it is observed that in the vicinity of the interface, the gradients of σ_{XX} and σ_{YY} with $\Delta T = -75$ K are greater than those with $\Delta T = 0$ K, and slightly higher than those with $\Delta T = 0$ K in the entire range of X. In contrast to those stress components, ε_{XX} with $\Delta T = -75$ K is lower than that with $\Delta T = 0$ K in the vicinity of the minimum point, being nearly equal to that with $\Delta T = 0$ K in the other region. This implies that the mismatch of the thermal expansion coefficients between the steel plate and SWNT/epoxy composite affects ε_{XX} not in the vicinity of the interface but near the minimum point.

Figure 12 shows the relationship between the D^* band shift and distance from the interface at strain levels of 3.0%, 3.5%, and 4%, which were observed using the strain gage attached in the uniform strain domain, as in Fig. 2. The D^* band shift has a peak point near $X = 0.1$ mm regardless of the strain level. The position of the peak point agrees with the minimum point of the stress and strain components in Fig. 11. This indicates that the D^* band shift substantiates the stress singularity field near the interface. Outside the stress singularity field, i.e., $X > 0.1$ mm, the D^* band shift increases with the approach of the interface from approximately $X = 5$ mm, where the deviation point from the uniform value of the D^* band shift agrees with that of ε_{XX} and not σ_{XX} as in Fig. 11. Thus, it is also confirmed that the D^* band shift corresponds to the variation of ε_{XX} under biaxial stress condition.

Using the linear relation between ε_{XX} (%) and the D^* band shift, Δv (cm^{-1}) in Fig. 6, we can convert the D^* band shift into the strain as follows:

$$\varepsilon_{XX} = -\frac{\Delta v}{28.74}. \tag{3}$$

Figure 13 shows the ε_{XX} distributions converted from the D^* band shift distributions in Fig. 12 using Eq. 3 together with the analytical ones, where both the experimental and analytical strains are normalized using the value of the strain at $X = 10$ mm. In the vicinity of the minimum point, the analytical plots with $\Delta T = -75$ K are nearly equal to the upper limits of the experimental ones, whereas those with $\Delta T = 0$ K are higher than the experimental ones. In the region except near the minimum point, the experimental

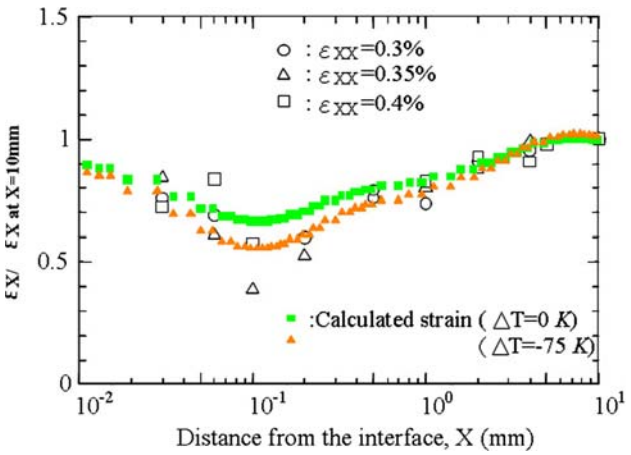

Fig. 13 Comparison between observed and calculated strain distributions along the center of the specimen

plots almost agree with the analytical ones for both $\Delta T = 0$ and -75 K. This implies that there is a considerable residual stress due to the mismatch of thermal expansion coefficients and that the rigidity of the SWNT/epoxy composite does not vary in the region that the distance from the interface is greater than 0.03 mm.

In the vicinity of the metal/polymer interface, chemical or physical conversions will occur and induce a gradient of residual stress and rearrangement of polymeric structures; a third layer called "interphase", that has chemical, physical, and mechanical properties different from those of the bulk polymeric material, is formed between the metal and polymeric substrate [18]. If the interphase thickness is greater than 1/10 of the polymeric layer, the mechanical properties of the interphase layer should be taken the stress analysis of the metal/polymer bonding material into consideration. To evaluate the thickness of the interphase layer, several experiments have been reported. From the measurements of the rigidity of the adhesive layer or coating layer on a metal plate in various thicknesses, some studies showed that the rigidity of the polymeric layer still varies with the layer thickness greater than or equal to 0.1 mm [19–21]. Other investigators reported that the interphase layer does not appear on such a scale [22, 23]. In most of these experimental studies, the strains in the polymeric layer are obtained using mechanical devices for measurement of the relative displacement of the specimen, wherein the calculated strains are of the mean values through the polymeric layer and therefore require the correction of displacement of the metallic substrate.

Such a polymeric layer at the metal/polymer interface is extremely thin and also the relative displacement is very small. A measurement system with a high sensitivity and a large measuring range is thus required to determine the strain accurately, though it is difficult to satisfy these two demands at the same time. Thus, the local measurements of the strain, elastic modulus, hardness, and so on in the polymeric layer are necessitated to evaluate the interphase thickness. Such measurements have been rarely conducted: Lilleheden measured strain distributions in an adhesive layer of an aluminum joint by Moiré interferometry, and the observed results indicated that the rigidity of the adhesive layer was kept constant in the layer thickness greater than 0.16 mm [5]. Recently, the elastic modulus distributions in the adhesive layer have been estimated by nanoindentation [24, 25]: One study indicated that the interphase layer thickness of a CFRP adhesive joint was less than 0.03 mm [24], whereas for an aluminum adhesive joint, it has been reported that some chemical surface treatment extended the interphase thickness up to 0.07 mm [25]. The former result agrees with our experimental trend, though the steel surface for bonding was treated only by grit blasting. It is unclear whether such a thick interphase layer appears following a chemical treatment or not. In conclusion, the present measurement method is useful for estimating the mechanical properties in the vicinity of the interface.

Conclusions

Strain distributions near the steel/epoxy bonded interface were measured by micro-Raman spectroscopy under uniaxial tensile loading condition, where the SWNTs were dispersed in the epoxy resin as mechanical sensors and the D^* band shift was used to monitor the strain. The main conclusions are summarized as follows:

1. The D^* band shift of an epoxy/SWNT composite was measured under biaxial stress condition using a cruciform-type specimen. It is confirmed that the D^* band shift can be used to measure the strain in the polarized direction even though under biaxial stress condition.
2. The distributions of the D^* band shift near the epoxy/steel bonded interface were determined using steel/SWNT composite joints under uniaxial tensile loading condition, and then the D^* band shifts were converted to strains of the epoxy phase. The measured strain distributions were compared with those calculated by finite-element analysis. Experimental results indicate that the strain singularity appears in the vicinity of the interface, similar to the results of the finite-element analysis, and that the analytical plots with $\Delta T = -75$ K are nearly equal to the upper limits of the experimental ones in the vicinity of the minimum point, whereas those with $\Delta T = 0$ K are lower than the experimental ones. In the region except near the minimum points, the experimental plots almost agree with the analytical ones for both $\Delta T = 0$ and -75 K. This implies that there is a considerable residual stress owing to the mismatch of thermal expansion coefficients and that the rigidity of the SWNT/epoxy composite does not vary in the region that the distance from the interface is greater than 0.03 mm.

Acknowledgements The authors would like to thank Dr. T. Miyake and Mr. M. Futamura of Nagoya Municipal Research Institute for their valuable suggestions concerning the Raman spectra measurement, Dr. J. Kadota of Osaka Municipal Technical Research Institute for his helpful support in the preparation of SWNT composites, and Drs. Y. Fukuchi and Y. Kitagawa of the Industrial Research Institute of Hyogo Prefecture for their helpful advice and comments on the finite-element analysis.

References

1. Bogy DB (1971) J Appl Mech 38:377
2. Hattori T, Sakata S, Murakami G (1989) J Electron Packag 111:243

3. Hutchinson JW, Suo Z (1992) Adv Appl Mech 29:64
4. Reedy ED Jr (1990) Eng Fract Mech 36:575
5. Lilleheden L (1994) Int J Adhes Adhes 14:32
6. Lourie O, Wagner HD (1998) J Mater Res 13:2481
7. Wood JR, Zhao Q, Wagner HD (2001) Compos A 32:391
8. Zhao Q, Frogley MD, Wagner HD (2001) Compos Sci Technol 61:2139
9. Frogley MD, Zhao Q, Wagner HD (2002) Phys Rev B 65:113413
10. Zhao Q, Wagner HD (2003) Compos A 34:1219
11. Kao CC, Young RJ (2004) Compos Sci Technol 64:2291
12. Lucas M, Young RJ (2004) Compos Sci Technol 64:2297
13. Lucas M, Young RJ (2004) Phys Rev B 69:085405
14. Zhao Q, Wagner HD (2004) Trans R Soc Lond A 362:2407
15. Barber AH, Zhao Q, Wagner HD, Bailli CA (2004) Compos Sci Technol 64:1915
16. Krenchel H (1964) Fiber reinforcement. Akademisk, Copenhagen
17. Fidelus JD, Wiesel E, Gojony FH, Sculte K, Wanger HD (2005) Compos A 36:1555
18. Mittal KL (1978) In: Mittal KL (ed) Adhesion measurement of thin films. ASTM STP 640, American Society Testing Materials, Philadelphia, p 5
19. Peretz D (1978) J Adhes 9:115
20. Brinson HF (1982) Composite 13:377
21. Bouchet J, Roche AA, Jacqelin E (2001) Thin Solid Films 15:321
22. Jeandreau JP (1986) Int J Adhes Adhes 6:229
23. Adams RD, Coppendale J (1977) In: Allen K (ed) Adhesion 1. Applied Science Publishers, London, pp 1–17
24. Zheng S, Ashroft IA (2005) Int J Adhes Adhes 25:67
25. Brodynski A, Geis PL, Kopnarski M, Passlack S, Presser M, Vogt D (2008*)* Proceedings of 31st Annual Meeting of The Adhesion Soc. Inc., p 85